Structure of strongly coupled multicomponent plasmas

K. Wünsch,[1] P. Hilse,[2] M. Schlanges,[2] and D. O. Gericke[1]
[1]*Centre for Fusion, Space and Astrophysics, Department of Physics, University of Warwick, Coventry CV4 7AL, United Kingdom*
[2]*Institut für Physik, Ernst-Moritz-Arndt-Universität Greifswald, Felix-Hausdorff-Straße 6, 17487 Greifswald, Germany*
(Received 30 November 2007; revised manuscript received 2 March 2008; published 12 May 2008)

We investigate the short-range structure in strongly coupled fluidlike plasmas using the hypernetted chain approach generalized to multicomponent systems. Good agreement with numerical simulations validates this method for the parameters considered. We found a strong mutual impact on the spatial arrangement for systems with multiple ion species which is most clearly pronounced in the static structure factor. Quantum pseudopotentials were used to mimic diffraction and exchange effects in dense electron-ion systems. We demonstrate that the different kinds of pseudopotentials proposed lead to large differences in both the pair distributions and structure factors. Large discrepancies were also found in the predicted ion feature of the x-ray scattering signal, illustrating the need for comparison with full quantum calculations or experimental verification.

DOI: 10.1103/PhysRevE.77.056404 PACS number(s): 52.27.Gr, 52.70.−m, 52.59.Hq

I. INTRODUCTION

Modern pulsed-power technology has opened the way to investigate dense strongly coupled plasmas in the laboratory. Other examples for strongly interacting particles are the dust grains in complex plasmas or ions in traps. These systems exhibit a short-range fluidlike structure that might be considered as the most striking difference to traditional gaslike plasmas. This well-pronounced structure, particularly in the ionic subsystem, affects many equilibrium, transport, and relaxation properties. This is well known for the equation of state [1,2], the Ziman formula for the conductivity [3], and the equilibration of two-temperature plasmas [4]. Precise structural information is also needed for the interpretation of x-ray diffraction measurements [5], the newly developed diagnostics by means of spectrally resolved x-ray Thomson scattering [6–10], and the elastic scattering measurements presented in Ref. [11].

The short-range order in the ion component of strongly coupled plasmas is created by the strong Coulomb interaction whose strength is usually cast by the classical coupling parameter

$$\Gamma_{ii} = \frac{Z_i^2 e^2}{a_i k_B T}, \tag{1}$$

where $a_i = (3/4\pi n_i)^{1/3}$ is the mean interparticle spacing. Gaslike plasmas with $\Gamma_{ii} \ll 1$ have almost uncorrelated particles and show no structure. For strongly coupled ions with $\Gamma_{ii} > 1$, the correlations exceed the thermal energy and a short-range order is established. The structural properties become increasingly significant with coupling strength. Eventually, the ions freeze into a lattice for $\Gamma_{ii} > 172$ [12]. The electrons, on the other hand, are almost always weakly coupled, but very dense systems exhibit a short range order due to the Pauli principle (see, e.g., Ref. [13]).

Intrinsically, plasmas contain at least two components (electrons and ions) and most systems have more than one ion species due to multiple chemical elements and/or ionization stages. In contrast, the theoretical approaches for the structural properties consider mostly only one ion component at an average charge state using either the one-component plasma (OCP) or the Yukawa model [1]. The first considers the electrons only as a rigid neutralizing background, while the second allows for polarization of the electron gas, resulting in statically screened ion-ion interactions. The advantages of such a treatment are a largely reduced numerical effort and the fact that the results depend on only one or two parameters: namely, the coupling parameter Γ or the coupling and screening parameters Γ and κ, respectively.

The OCP and Yukawa models have been intensively investigated by classical Monte Carlo (MC) [14–16] and molecular dynamics (MD) [12,17] simulations which can precisely predict the ionic structure, but require a large numerical effort. A computationally less demanding approach is based on integral equations developed in fluid theory [18,19]. For the Coulomb systems considered, this hypernetted chain (HNC) approach has been shown to yield good results compared to simulations for coupling parameters up to $\Gamma \approx 100$ [20]. As for the simulations, this method has been mainly applied to the OCP and Yukawa models; only few calculations were applied to ionic mixtures [21,22], electrons and ions [23,24], and atomic-molecular hydrogen [25].

The techniques mentioned above are based on classical physics and are appropriate for ions only. To treat electrons correctly, quantum effects must be included. This can be approximately achieved by using quantum pseudopotentials which are designed to model the quantum behavior in classical calculations [23,26–29]. However, the applicability of these potentials is limited to weakly degenerate electrons. Otherwise, a full quantum approach such as the Green's function technique [30], path integral Monte Carlo simulations [31–33], or density functional molecular dynamics simulations [34,35] should be applied. However, these techniques are computationally even more demanding than classical simulations.

In this paper, we will investigate the structure of multicomponent plasmas mainly through the integral equation approach of classical fluid theory. In addition, MD and MC simulations were used to validate the results. The numerical HNC scheme is extended to allow for an arbitrary number of components. This enables us to study plasmas with multiple ion species as well as to go beyond the linear response ap-

proximation for the electrons. Quantum effects are included by different pseudopotentials that mimic quantum diffraction as well as exchange. In particular, the different electron-ion potentials suggested generate large differences for the pair distributions and static structure factors. The multicomponent code is then used to study exchange potentials that act only on like-spin electrons and, therefore, requires two electron components. Beryllium in the warm dense matter regime was chosen as the main example since it was investigated in recent experiments by x-ray scattering [7,9]. All input parameters needed for our calculations—i.e., electron density, ion charge state, and temperature—have been inferred from the experiments. Using these values, the theoretically obtained structure factors, particularly for small wave numbers, show considerable differences depending on the number of components and the kind of pseudopotential used.

II. THEORETICAL DESCRIPTION

A. Basic definitions and weak coupling

The spatial arrangements in systems of classical particles are usually described by density correlations which in turn define the pair distribution function via

$$g_{ab}(\mathbf{r}_1,\mathbf{r}_2) = \frac{1}{n_a n_b}\left\langle \sum_{\substack{i=1 \\ i\neq j \ \forall \ a=b}}^{N_a} \sum_{j=1}^{N_b} \delta(\mathbf{r}_1-\mathbf{r}_i)\,\delta(\mathbf{r}_2-\mathbf{r}_j)\right\rangle, \quad (2)$$

where $\mathbf{r}_i$ and $\mathbf{r}_j$ are the positions of the particles and the brackets denote the average over a canonical ensemble. In fluidlike systems, the pair distribution function (and all other correlation functions) depends only on the interparticle spacing $r=|\mathbf{r}_1-\mathbf{r}_2|$. Equivalently, the structure of the system can also be depicted by the static structure factor which is defined via the Fourier transformation of the total correlation function $h_{ab}(r)=g_{ab}(r)-1$ —that is,

$$S_{ab}(\mathbf{k}) = \delta_{ab} + \sqrt{n_a n_b}\int d\mathbf{r}[g_{ab}(r)-1]\exp(i\mathbf{k}\cdot\mathbf{r}). \quad (3)$$

In weakly coupled systems described by pair potentials $V_{ab}(r)$, the interactions can be treated within the linear response and the pair distribution is given by [1]

$$g^0_{ab}(r) = \exp\{-\beta V_{ab}(r)\}, \quad (4)$$

where $\beta=1/k_BT$ denotes the inverse temperature. It is well known that the long-range nature of the Coulomb force leads to screening. As a result, the bare Coulomb potential in expression (4) must be replaced by the screened Coulomb or Debye potential [2]

$$V^D_{ab}(r) = \frac{Z_a Z_b e^2}{r}\exp(-\kappa r), \quad (5)$$

where κ is the inverse screening length. If only the electrons are treated within the linear response, the Yukawa model for ions interacting via the statically screened potential (5) follows. To allow for (partially) degenerate electrons needed to describe warm dense matter, the inverse electron screening length is given by

$$\kappa_e^2 = \frac{4e^2 m_e}{\pi\hbar^3}\int_0^\infty dp\, f_e(p), \quad (6)$$

where $f_e(p)$ is the Fermi distribution for the electrons. This definition includes the Debye and Thomas-Fermi screening models as limiting cases for classical and highly degenerate electrons, respectively.

B. Hypernetted chain approach (HNC)

The weak-coupling approximation (4) fails for denser and more strongly coupled plasmas, where the correlations cannot be treated as a small perturbation of the thermal motion. Here, higher-order correlations must be taken into account which can be done using the integral equation approach of fluid theory. For that goal, one introduces the direct correlation function $c_{ab}(r)$ [18,19] which is connected to the total correlation function $h_{ab}(r)$ via the Ornstein-Zernike relation [36]:

$$h_{ab}(\mathbf{r}) = c_{ab}(\mathbf{r}) + \sum_c n_c \int d\bar{\mathbf{r}}\; c_{ac}(\bar{\mathbf{r}})h_{cb}(|\mathbf{r}-\bar{\mathbf{r}}|). \quad (7)$$

Furthermore, we need a closure relation to fully determine the system. Here, we use the hypernetted chain closure relation that is known to reproduce numerical simulation data for one-component Coulomb systems well:

$$g_{ab}(r) = \exp[-\beta V_{ab}(r) + h_{ab}(r) - c_{ab}(r)]. \quad (8)$$

The two equations (7) and (8) fully define the static structure in classical multicomponent systems. For the numerical evaluation, it is useful to consider the fact that the Ornstein-Zernike relation (7) contains a convolution and is therefore algebraic in Fourier space. In the case of one component, the HNC equations (7) and (8) can thus be easily solved by iteration going back and forth from real to Fourier space and vice versa. For the systems with N components, the structure of the equations is a bit more complicated since we have to consider $N(N+1)/2$ different correlation functions (note the symmetry $h_{ab}=h_{ba}$ and $c_{ab}=c_{ba}$). The Ornstein-Zernike relation is therefore a matrix equation in Fourier space:

$$\tilde{H}(k) = \tilde{C}(k) + \tilde{C}(k)\tilde{D}\tilde{H}(k), \quad (9)$$

with $\tilde{D}=\delta_{ab}n_a$ containing the densities of the different species and $\tilde{C}(k)$ and $\tilde{H}(k)$ having elements $c_{ab}(k)$ and $h_{ab}(k)$, respectively. For a two-component system, this equation can be solved simply by the Kramers rule while one has to rely on numerical matrix inversion for the general multicomponent case.

Since the screening is described within the multicomponent HNC scheme, the two-body potentials used for the interacting plasma particles must be Coulomb-like for long distances. Accordingly, the direct correlation function is also long ranged:

$$\lim_{r\to\infty} c_{ab}(r) = -\beta V_{ab}(r) \sim \frac{1}{r}. \quad (10)$$

This behavior prohibits a direct Fourier transformation which can, however, be achieved by introducing short-range func-

tions similar to Ref. [37]. We can now solve the resulting system of equations iteratively starting with the weak-coupling solution (10). After transformation to short-range functions and into Fourier space, we solve the Ornstein-Zernike relation (9) by numerical matrix inversion for each k value. The resulting matrices $\tilde{C}(k)$ are then reassembled into functions $c_{ab}(k)$ and transformed back to real space. Here, the closure relation (8) is used to calculate new total correlation functions $h_{ab}(r)$. These newly obtained functions are now used as an improved guess at the start of the loop until convergence is achieved. For the transformations between real and Fourier space, we employ a fast Fourier transformation (FFT) which has been, as the matrix inversion techniques, implemented from Ref. [38].

The iterative procedure above is practically limited by the coupling strength as expressed in the Coulomb coupling parameter Γ. For systems with purely repulsive forces, such as the ion components in a plasma, the full fluid region is accessible. In contrast, the attractive electron-ion interaction poses a considerable problem which is mitigated by the use of weaker pseudopotentials that are employed to mimic quantum effects in classical systems (see Sec. III B). Such a treatment allows HNC solutions up to moderately coupled plasmas with $\Gamma_{ee}=e^2/a_e k_B T \approx 1$.

C. Numerical simulations

Complementary to the HNC calculations, classical MC and MD simulations were applied to obtain the structural properties. The simulations were mainly used to verify the accuracy of the HNC results since they intrinsically include all correlations, especially the bridge diagrams neglected in the HNC approach. All simulations were performed with several thousand electrons and ions contained in a cubic volume with periodic boundary conditions. The obtained particle positions define the pair distributions g_{ab} directly via definition (2) where the average was taken over many configurations or times, respectively, to reduce the numerical noise.

For the MC simulations, the well-known Metropolis algorithm was implemented and good agreement with the HNC approach was found for weakly to moderately coupled plasmas. However, we were unable to find a stable solution for strongly coupled electron-ion systems.

In contrast, multicomponent molecular dynamics simulations gave stable solutions even for strong coupling. Here, the very different time scales for the dynamics of electrons and ions are a well-known problem of such dynamic calculations. For the static structure aimed for in this paper, it can be avoided by using an artificial mass ratio. The reason is the ergodicity of the system which leads to the fact that static correlations depend only on the interplay of potential and kinetic energies. This can also be seen in the HNC scheme which shows no reference to particle mass. Test runs with different mass ratios confirmed this statement. Using similar masses, one obtains well-sampled pair distributions for all combinations of species and acceptable run times.

III. RESULTS AND DISCUSSION

A. Strongly coupled ion systems

Let us first consider the free plasma electrons within linear response and investigate plasmas with multiple ion species. The ion-ion interaction is then given by a screened Coulomb potential (5). Plasmas with different ionization stages and systems containing more than one element such as plastics (CH) or SF_6 are typical examples.

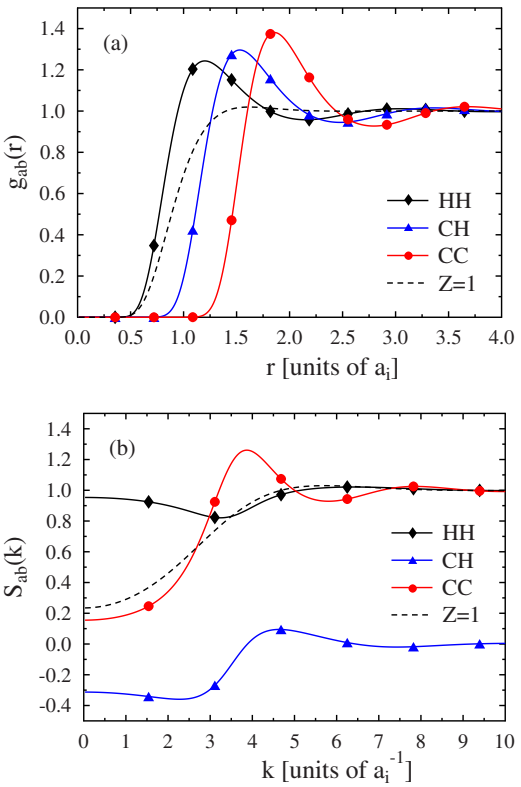

FIG. 1. (Color online) (a) Partial pair distributions for a CH plasma with $n_H=n_C=2.5\times10^{23}$ cm^{-3} and $T=2\times10^4$ K. The hydrogen and carbon ions are fully and fourfold ionized, respectively. For comparison, the dashed line, labeled $Z=1$, shows results for an isolated hydrogen plasma under the same conditions. (b) Static structure factors for the same CH plasma.

Figure 1 shows the partial ion-ion pair distributions and structure factors of a strongly coupled CH plasma. In this example, all three partial pair distributions show a typical signature for strongly coupled plasmas: one or more maxima indicating a high probability to find the next ion at some distance and a depleted area (the so-called correlation hole) in the vicinity of each ion. Since the carbon-carbon coupling is the strongest, the corresponding pair distribution and structure factor show more pronounced maxima.

The well-established short-range structure for the protons demonstrates the need for a coupled multicomponent description. For comparison, Fig. 1 shows also data for a one-component plasma of singly charged ions at the same conditions. Clearly, such a plasma is only moderately coupled which results in a monotonic increase of both the pair distribution and the structure factor. Comparison with the CH plasmas shows that the more highly charged carbon ions imprint their structure onto the subsystems of the protons. Neither a two-fluid description nor an average charge state calculation can reproduce such a behavior. It was suggested that the observed smaller average spacing of the protons or, in this case, deuterons due to the presence of more highly

charged ions could enhance the nuclear reaction rates in multicomponent astrophysical plasmas [22].

The structure factors at small k values show the need for a fully coupled description even more clearly. While the carbon-carbon structure factor roughly reflects the behavior of a one-component calculation, both other partial structure factors show clear signs of modulation: the carbon-proton structure factor exhibits the maximum at the same position than the carbon-carbon one which indicates an alternating arrangement of carbon ions and protons. For large k, the proton-proton structure follows the one for an isolated proton systems, but it is much larger in the hydrodynamic limit—i.e., at small k. This reflects the fact that the long-range part of the proton-proton potential is strongly altered by the carbon ions. Since the HNC scheme self-consistently includes the screening contribution of all species considered, the form of $S_{HH}(k)$ can be interpreted as a strong nonlinear screening effect generated by the carbon ions. Note that the partial structure factor S_{ab} with $a \neq b$ is defined as the Fourier transform of $h_{ab}=g_{ab}-1$ without adding unity. That may lead to negative values of these partial structure factors at small k. However, scattering probabilities are proportional to the total structure factor—that is, positive definite—and, due to this definition, have the correct limit $\lim_{k\to\infty} S(k)=1$.

Similar effects, but weaker, can be found in plasmas with one element but multiple ionization stages. As an example, compressed gold with an equal number of singly and doubly charged ions is considered in Fig. 2. In this two-component plasma (TCP), the screening produced by the electrons is rather strong as indicated by an inverse screening length of $\kappa_e=1.81a_i^{-1}$.

Such systems are often described by an average charge state for the ions ($\bar{Z}=1.5$ in this case). To estimate the error produced by such a calculation, we defined the average ionic pair distribution by

$$\bar{g}(r) = \frac{1}{N^2}\sum_{ab} g_{ab}(r), \tag{11}$$

where N is the number of components. The average structure factor is given in the usual way by the Fourier transformation of $\bar{g}-1$. These quantities are then compared to the one from a one-component calculation using an average charge state $\bar{Z}$. The comparison in Fig. 2 shows that the assumption of an average charge state overestimates the coupling strength [steeper slope of $g(r)$, larger correlation hole, and more pronounced peaks]. Moreover, the ion-ion structure factor at small k values is underestimated. These large relative differences are very important for the interpretation of the x-ray scattering signals where $S_{ii}(k)$ for small k is needed.

In addition to the examples shown, we performed calculations for other multicomponent systems such as other plastics and SF_6 which all showed the same behavior as the presented cases. In other tests for dusty plasmas with more than 100 different charge states for different dust grain species, we could not find any hints that would limit the ability of the method (other than run time).

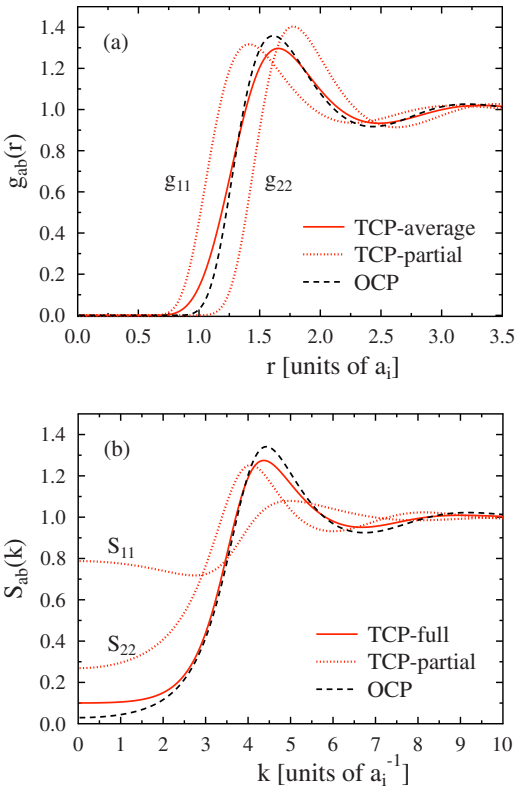

FIG. 2. (Color online) (a) Partial pair distributions (dotted) for a gold plasma with $n_i=10^{24}$ cm^{-3}, $T=10^4$ K, and ion charge states of $Z=1$ and $Z=2$ (equally distributed). The solid line shows the averaged pair distribution (11) and the dashed line the results of a one-component calculation with $\bar{Z}=1.5$. (b) Same as (a) for the static structure factor.

B. Electron-ion systems: Quantum diffraction effects within the classical description

The HNC approach is a powerful technique to describe classical plasmas in the strongly coupled region. It can also be used to go beyond the linear screening model by considering the electrons within a multicomponent version and thereby treat electrons and ions on an equal footing. The quantum mechanical nature of the electrons—e.g., quantum diffraction as well as exchange effects—must, however, be included in this classical scheme. The diffraction effects, which will be considered first, can be even important in the nondegenerate high-temperature region.

One way to include quantum effects approximately is based on the use of pseudopotentials that are designed to mimic certain quantum effects within the classical method (HNC or simulations). Such a quantum potential can be obtained by identifying the two-particle Slater sum $\hat{S}_{ab}$ with an auxiliary quantum potential in the classical partition sum [39,41]:

$$\hat{S}_{ab}(r) = \exp[-\beta V_{ab}^{\mathrm{qm}}(r)]. \tag{12}$$

Since we are interested in the description of a system with free electrons, only the scattering states should be included in the Slater sum. By treating the Coulomb interaction on the

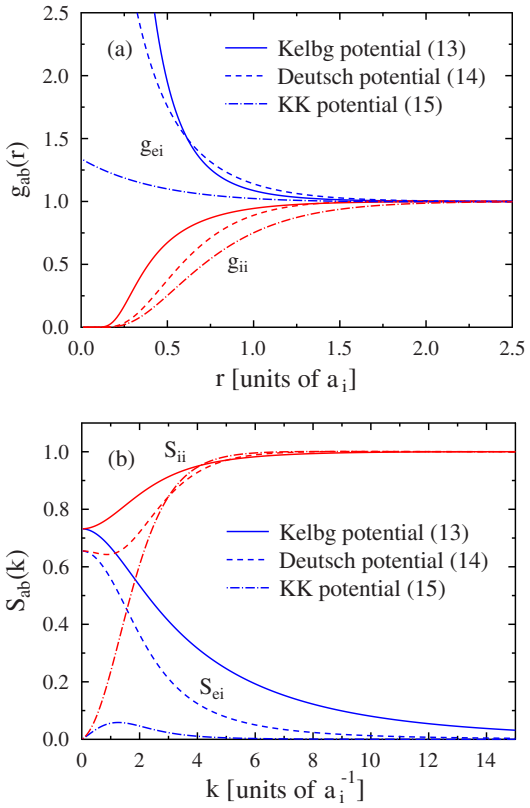

FIG. 3. (Color online) (a) Electron-ion (upper triple) and ion-ion (lower triple) pair distributions for a plasma with $n_i=10^{22}$ cm^{-3}, $Z=1$, and $T=4.5\times10^4$ K. Different quantum pseudopotentials are used for the *e-i* and *e-e* interactions as labeled. In the case of the KK potential (15), the *e-e* interaction is described by the Deutsch potential (14). *i-i* interactions are always described by the Coulomb potential. (b) Same as (a) for the static structure factors.

level of a first Born approximation, the Kelbg potential follows [26,27]:

$$V_{ab}^{\text{Kelbg}}(r)=\frac{Z_aZ_be^2}{r}\{1-e^{-x_{ab}^2}+\sqrt{\pi}x_{ab}[1-\Phi(x_{ab})]\}. \quad (13)$$

Here, $x_{ab}=r/\lambda_{ab}$ where $\lambda_{ab}=[\hbar/(2\mu_{ab}k_BT)]^{1/2}$ is the thermal de Broglie wavelength with reduced mass $\mu_{ab}=m_am_b/(m_a+m_b)$ and $\Phi(x)=(2/\sqrt{\pi})\int_0^x dt\,\exp(-t^2)$ denotes the error function.

Other forms for quantum diffraction potentials were suggested by Deutsch [28],

$$V_{ab}^{\text{Deutsch}}(r)=\frac{Z_aZ_be^2}{r}\left[1-\exp\left(-\frac{r}{\lambda_{ab}}\right)\right], \quad (14)$$

and Klimontovich and Kraeft (KK) [24,29],

$$V_{ei}^{\text{KK}}(r)=-\frac{k_BT\xi_{ei}^2}{16}\left[1+\frac{k_BT\xi_{ei}^2}{16Ze^2}r\right]^{-1}, \quad (15)$$

where $\xi_{ei}=Z_ie^2\beta/\lambda_{ei}$. It should be mentioned that the last potential was derived in this form for the electron-ion interaction only.

All these potentials display a similar behavior: for large distances, they coincide with the Coulomb potential whereas they approach a finite value for $r\to0$. In this way, the singularity of the Coulomb potential at the origin is lifted. The amplitude of the potential at $r=0$ is, however, very different.

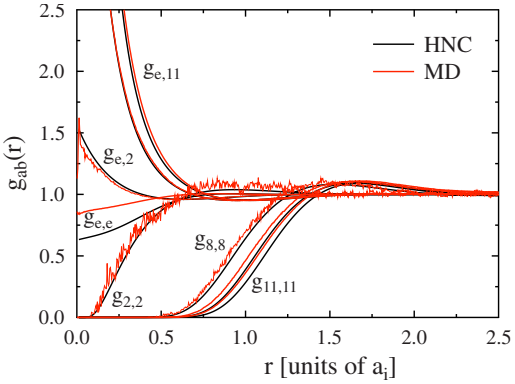

FIG. 4. (Color online) Comparison of the HNC results with molecular dynamics simulations for a plasma that contains different ion species: Xe^{11+} with $n_i=7.5\times10^{23}$ cm^{-3}, Xe^{10+} with $n_i=3\times10^{23}$ cm^{-3}, Ar^{8+} with $n_i=5\times10^{22}$ cm^{-3}, and He^{2+} with $n_i=5\times10^{23}$ cm^{-3}. The plasma temperature is $T=2.5\times10^6$ K. Shown are the functions g_{ee} and g_{ei} and the partial pair distributions for like ions, g_{aa}. The pair interactions are modeled by the Deutsch potential (14).

Figure 3 demonstrates the effect of the different quantum potentials on the predicted partial pair distributions and structure factors; both display large differences for small r and k, respectively. The changes in the ion-ion pair distribution g_{ii} and structure factor S_{ii} are quite indirect since for the ions quantum effects are negligible and, therefore, the ion-ion potential is pure Coulomb. The strongest potential (Kelbg) leads to an electron-ion pair distribution that is highly peaked around the origin. In turn, the electrons screen the ions very effectively and the resulting effective ion-ion potential is weakest. On the other hand, the very weak Klimontovich-Kraeft potential leads to almost no screening and accordingly to an OCP-like behavior of the ions which is highlighted by a very low value of $S_{ii}(0)$.

To demonstrate the abilities of the HNC code developed, Fig. 4 shows a comparison with molecular dynamics simulations data for an ionized gas mixture that contains four different ion species (two charge states of xenon, one for argon, and fully ionized helium). The electrons are also fully included in the code that thus has to describe five independent species. Except for the electron-electron distribution, we found an excellent agreement between HNC results and simulation data. The differences in $g_{ee}(r)$ at small r result from the fact that the electron-electron interaction is strong for these distances and the bridge diagrams neglected in the HNC approach matter here. Such differences between HNC and MD are well known for strongly coupled Coulomb systems [20]. The two approaches have two further distinctions: the HNC code is several orders of magnitude faster and noise due to poor statistics as in MD (some ion species are represented by a small number of ions only) is no issue. The latter is most prominent for the helium-helium pair distribution where the MD data are rather noisy.

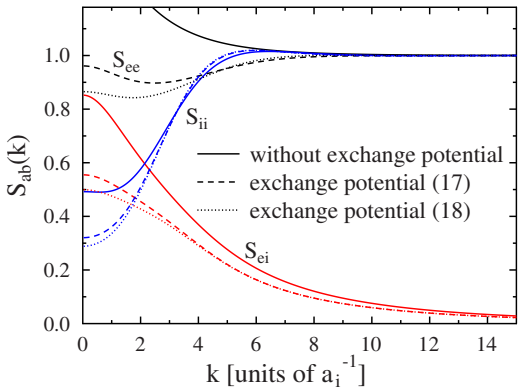

FIG. 5. (Color online) Partial structure factors for an aluminum plasma with $n_i=2.7\times10^{22}$ cm^{-3}, $Z=3$, and $T=1.5\times10^5$ K. The line styles correspond to different approximations for the *e-e* exchange potential; the diffraction part and the *e-i* interactions are described by the Deutsch potential (14) (Coulomb for *i-i* interactions).

C. Degenerate electrons: Modeling exchange

In addition to diffraction effects, quantum exchange contributions must be considered for high-density plasmas and the warm dense matter region. Exchange effects are usually modeled by adding a further term to the basic electron-electron potential that already considers diffraction effects:

$$V_{ee}^{\text{total}}(r) = V_{ee}^{\text{diff}}(r) + V_{ee}^{\text{ex}}(r). \tag{16}$$

These exchange contributions can be derived as for the case of quantum diffraction [40]. A different way is based on the known partition function for ideal systems. Considering two separate electron species, the potential between like-spin electrons is then given by [41]

$$V_{\uparrow\uparrow,\downarrow\downarrow}^{\text{ex}} = -k_B T \ln\left[1 - \exp\left(-\frac{2\pi r^2}{\lambda_{ee}^2}\right)\right]. \tag{17}$$

Of course, no exchange potential must be introduced between the two electron species. Such a treatment requires, however, one species more in the HNC equations or the simulation. Therefore, a spin-averaged potential is often used to simplify matters [42,43]:

$$V_{ee}^{\text{ex}} = k_B T(\ln 2)\exp\left[-\frac{1}{\pi \ln 2}\left(\frac{r}{\lambda_{ee}}\right)^2\right]. \tag{18}$$

One should, however, keep in mind that the potentials (17) and (18) do not describe systems that are highly degenerate and strongly coupled. The combination of both effects is treated only in an approximate way.

For most weakly degenerate plasmas, the pair distributions calculated using the exchange potentials (17) and (18) show only small differences (except g_{ee}). These potentials result, however, in slightly different screening which is magnified at the structure factors at small k. The neglect of exchange effects can lead to significant differences both in the pair distribution functions and in the static structure factors. Figure 5 demonstrates this fact for the case of an aluminum plasma that is moderately degenerate. Interestingly, even the ion-ion structure factor $S_{ii}(k)$ shows marks that stem from exchange. Again, the low k values, where differences are largest, are most relevant for the interpretation of the spectrum of x-ray scattering in the collective regime [9].

IV. APPLICATION TO X-RAY SCATTERING

A. Description of the scattering signal

The scattering of x rays, in particular Thomson and Compton scattering, is an emerging powerful diagnostics method well suited for dense plasmas and warm dense matter [6,7,9]. It exploits the fact that the intensity of the scattered light is proportional to the density-density structure factor of the electrons. For partially ionized matter, it is convenient to split the electrons into bound and free, where the last kind also includes the electrons of the screening cloud. Omitting internal excitations, the total electron-electron structure factor can then be recast as [44,45]

$$S_{ee}^{\text{tot}}(k,\omega) = |f_i(k) + q(k)|^2 S_{ii}(k,\omega) + Z S_{ee}^0(k,\omega). \tag{19}$$

Here, $f_i(k)$ denotes the atomic or ionic form factor (contribution from bound electrons) and $q(k)$ is the density of the screening cloud in Fourier space. The first term describes the scattering of the electrons comoving with the ions, while the second is the free-electron response. Up to now the ion peak cannot be spectrally resolved in the experiment and can therefore be treated statically. The contribution from the screening electrons can also be calculated by static structure factors [45]: $q(k)=\sqrt{Z}S_{ei}(k)/S_{ii}(k)$. All quantities needed to describe the ion peak are thus defined by the static structure discussed in this paper. The experimentally relevant k vector is defined by the wavelength of the probe radiation λ_0 and the scattering geometry via

$$k = \frac{4\pi}{\lambda_0}\sin(\theta/2), \tag{20}$$

where θ is the scattering angle.

B. Results and discussion

Figure 6 shows results for the structure factors using different quantum pseudopotentials discussed in the previous section. One obtains clearly quite different results depending on the choice for the potential. These differences occur for small to intermediate r in the pair distribution as well as for small k in the structure factors. The last fact highlights that the choice of the quantum potential also alters the long-range screening properties. Although the ion-ion potential is here Coulomb, this indirectly affects the ion-ion pair distribution and structure factor. One should, however, keep in mind that the pseudopotentials used here were derived for systems with weak quantum effects. Thus, the method of quantum potentials is quite overstretched in the case of Fig. 6 due to the highly degenerate electrons. This becomes particularly clear considering the kinetic energy: while the HNC approach uses Boltzmann statistics and therefore $\langle E_{\text{kin}}\rangle=\frac{3}{2}k_B T$, it should be replaced by the Fermi energy for highly degenerate systems.

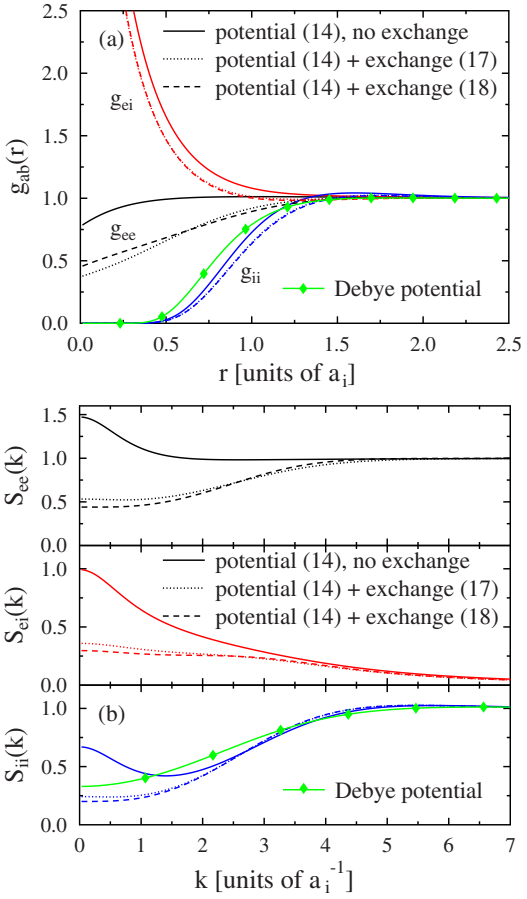

FIG. 6. (Color online) Comparison of the results from a multicomponent HNC approach using different quantum pseudopotentials for the conditions of recent x-ray scattering experiments [7] on beryllium with $n_i=1.23\times10^{23}$ cm^{-3}, $T=1.39\times10^5$ K, and $Z=2.2$. (a) Partial pair distributions and (b) structure factors.

The influence of a different treatment for the electrons on the ions can already be seen in the Yukawa model by using either a screening length calculated by the classical Debye formula or the Thomas-Fermi length applicable for highly degenerate electrons. For comparison, Fig. 6 displays the results of such a calculation where, in accordance with the general form (5) and the conditions of Fig. 6, an inverse screening length of $\kappa_e=2.16a_i^{-1}$ was used. The ions appear in this calculation more weakly coupled, which reveals that all pseudopotentials yield less effective screening than the linear screening model.

Tables I and II quantify the differences in the predicted weight of the ion peak [first term in Eq. (19)] for two different k values. These wave numbers correspond to a wavelength of the incident light of $\lambda_0=0.26$ nm and scattering angles of $\theta=160°$ (backward scattering) and $\theta=40°$ (forward scattering) applied to plasma conditions inferred from the experiments reported in Refs. [7] and [9], respectively. In addition, the screening function $q(k)$ was calculated within the classical linear response [46,47]

$$q(k)=\frac{-n_e\beta V_{ei}^C(k)}{\varepsilon_e(k,0)}=Z\frac{\bar{\kappa}_e^2}{\bar{\kappa}_e^2+k^2}, \tag{21}$$

where $\varepsilon_e(k,0)=k^2/(\bar{\kappa}_e^2+k^2)$ and the Coulomb potential $V_{ei}^C(k)=-4\pi Ze^2/k^2$ has been used in the second step. The quantities in the numerator can then be combined to the inverse of the classical Debye length which is denoted here by $\bar{\kappa}_e$ (electrons only) to mark the classical limits. In contrast to previous remarks, the dielectric function ε_e must be also used in the nondegenerate limit to ensure the boundary condition $\lim_{k\to0} q(k)=Z$.

The tables show once again that huge differences arise from the choice of the electron-ion potential, especially for small k. Particularly low weights are obtained using the Klimontovich-Kraeft potential (15) that results in a OCP-like behavior for the ions—i.e., very small values for $S_{ii}(0)$. The consideration of exchange contributions increases both $S_{ei}(k)$ and $S_{ii}(k)$ for small k which gives rise to an overall smaller weight of the ion peak. The consideration of two ion species changes the values slightly to higher values in both the linear response treatment and the calculations treating electrons within the HNC scheme.

TABLE I. Quantities needed to predict the height of the ion peak in the x-ray scattering signal. The material considered is beryllium at $n_i=1.23\times10^{23}$ cm^{-3}, $T=1.39\times10^5$ K, and an estimated charge state of $\bar{Z}=2.2$ which is probed at $k=4.76\times10^{10}$ m$^{-1}=5.97a_i^{-1}$. The following potentials are applied: K, Kelbg (13); D, Deutsch (14); D-ex, as D plus exchange term (18); KK, Klimontovich-Kraeft (15). Furthermore, the linear response approximation is applied (1C, one component; 2C, two components).

Potential used		$f_i(k)$	$S_{ei}(k)$	$S_{ii}(k)$	$q(k)$	$(f_i+q)^2S_{ii}(k)$
e-e	*e-i*					
D	D	1.46	0.078	1.024	0.113	2.53
D-ex	D	1.46	0.068	1.023	0.099	2.49
K	KK	1.46	0.007	1.022	0.010	2.21
D	KK	1.46	0.007	1.022	0.010	2.21
D-ex	KK	1.46	0.007	1.022	0.010	2.21
Linear response (1C)		1.46	-	1.009	0.336	3.25
Linear response (2C)		1.46	-	1.016	0.336	3.28

TABLE II. Same as Table I, but for a smaller wave number of $k=10^{10}$ m$^{-1}=1.25a_i^{-1}$.

Potential used		$f_i(k)$	$S_{ei}(k)$	$S_{ii}(k)$	$q(k)$	$(f_i+q)^2S_{ii}(k)$
e-e	*e-i*					
D	D	1.78	0.569	0.424	1.990	6.03
D-ex	D	1.78	0.263	0.262	1.489	2.80
K	KK	1.78	0.036	0.128	0.417	0.62
D	KK	1.78	0.048	0.130	0.548	0.71
D-ex	KK	1.78	0.036	0.130	0.411	0.62
Linear response (1C)		1.78	-	0.429	1.762	5.38
Linear response (2C)		1.78	-	0.325	1.762	4.08

A direct comparison of the results present in Tables I and II with experimental data is unfortunately not possible since the extraction of the corresponding weights of the ion peak from the published spectra is beyond the scope of this work. A theoretical model that uses the KK potential yields, however, good agreement with the scattering intensity measured [9]. Therefore, weights slightly less than unity can be extracted for the conditions of Table II. The KK potential is, however, the theoretically least justified quantum pseudopotential used. Accordingly, further experimental data or a full quantum description of the warm dense matter investigated seem to be required.

V. CONCLUSIONS

We investigated the structural properties of dense strongly coupled multicomponent plasmas using classical hypernetted chain equations and numerical simulations. Both methods, which yield very similar results, are typically applied for one- or two-component plasmas. By extending the approach to systems with an arbitrary number of components, we could demonstrate the shortcomings of the OCP and Yukawa calculations. Strongly coupled plasmas, which consist of different chemical components and have ions with very distinct charge states, cannot be described with such an OCP approach at all. Here, the ions with the highest charge state imprint their structure on the other components and a multicomponent version is absolutely necessary. This effect is less pronounced for plasmas with ions in successive charge states. However, we find here also quantitative discrepancies between multicomponent and one-component calculations in the strongly coupled region.

The generalization to many components allows us to study electron-ion systems treating electrons on the same footing as ions. In this case, we have to take quantum effects, which are intrinsic for the electrons, into account. Both quantum diffraction and exchange can be approximately modeled by quantum pseudopotentials. We tested different types of potentials and found large differences for the predicted pair distributions and structure factors in the warm dense matter region. Interestingly, calculations considering two electron components in different spin states yield in the region of moderate degeneracy significantly different results than those using a spin-averaged exchange potential.

We finally applied our structural calculation to x-ray scattering in warm dense matter. Here, the choice of the quantum potential can strongly affect the predicted height of the ion feature which is related to the static structure factors. This is particularly pronounced in the case of forward scattering while it is less important for backward scattering. These results suggest that scattering under large angles is better suited for plasma diagnostics since these results are nearly independent of the approximation applied. Due to much larger differences between the models for smaller k values, forward scattering seems, in contrast, to be the better approach for an experimental test of the theoretical predictions. Alternatively, the problems originating from the quantum pseudopotentials may be resolved by comparison with full quantum simulations.

ACKNOWLEDGMENTS

We thank Th. Bornath and W.-D. Kraeft (Rostock) for enlightening discussions on quantum pseudopotentials. In part, this work was supported by the Deutsche Forschungsgemeinschaft (Grant No. SFB 652). K.W. and D.G. acknowledge support from the Engineering and Physical Sciences Research Council (U.K.).

[1] J. P. Hansen and I. R. McDonald, *Theory of Simple Liquids* (Academic Press, London, 1990).

[2] D. Kremp, M. Schlanges, and W.-D. Kraeft, *Quantum Statistics of Nonideal Plasmas* (Springer, Berlin, 2005).

[3] J. M. Ziman, Philos. Mag. **6**, 1013 (1961).

[4] M. W. C. Dharma-wardana and F. Perrot, Phys. Rev. E **58**, 3705 (1998); **63**, 069901 (2001).

[5] D. Riley, N. C. Woolsey, D. McSherry, I. Weaver, A. Djaoui, and E. Nardi, Phys. Rev. Lett. **84**, 1704 (2000).

[6] G. Gregori, S. H. Glenzer, W. Rozmus, R. W. Lee, and O. L.

Landen, Phys. Rev. E **67**, 026412 (2003).
[7] S. H. Glenzer, G. Gregori, R. W. Lee, F. J. Rogers, S. W. Pollaine, and O. L. Landen, Phys. Rev. Lett. **90**, 175002 (2003).
[8] G. Gregori, S. H. Glenzer, H.-K. Chung, D. H. Froula, R. W. Lee, N. B. Meezan, J. D. Moody, C. Niemann, O. L. Landen, B. Holst, R. Redmer, S. P. Regan, and H. Sawada, J. Quant. Spectrosc. Radiat. Transf. **99**, 225 (2006).
[9] S. H. Glenzer, O. L. Landen, P. Neumayer, R. W. Lee, K. Widmann, S. W. Pollaine, R. J. Wallace, G. Gregori, A. Höll, Th. Bornath, R. Thiele, V. Schwarz, W.-D. Kraeft, and R. Redmer, Phys. Rev. Lett. **98**, 065002 (2007).
[10] H. Sagawa, S. P. Regan, D. D. Meyerhofer, I. V. Igumenshchev, V. N. Goncharov, T. R. Boehly, R. Epstein, T. C. Sangster, V. A. Smalyuk, B. Yaakobi, G. Gregori, S. H. Glenzer, and O. L. Landen, Phys. Plasmas **14**, 122703 (2007).
[11] A. Ravasio, G. Gregori, A. Benuzzi-Mounaix, J. Daligault, A. Delserieys, A. Ya. Faenov, B. Loupias, N. Ozaki, M. Rabec le Gloahec, T. A. Pikuz, D. Riley, and M. Koenig, Phys. Rev. Lett. **99**, 135006 (2007).
[12] S. Hamaguchi, R. T. Farouki, and D. H. E. Dubin, Phys. Rev. E **56**, 4671 (1997).
[13] V. S. Filinov, V. E. Fortov, M. Bonitz, and D. Kremp, Phys. Lett. A **274**, 228 (2000).
[14] H. Iyetomi, S. Ogata, and S. Ichimaru, Phys. Rev. A **46**, 1051 (1992).
[15] J. M. Caillol and D. Gilles, J. Stat. Phys. **100**, 905 (2000).
[16] J. P. Hansen, Phys. Rev. A **8**, 3096 (1973).
[17] P. Hartmann, G. J. Kalman, Z. Donko, and K. Kutasi, Phys. Rev. E **72**, 026409 (2005).
[18] J. M. J. van Leuwen, J. Groenveld, and J. DeBoer, Physica (Amsterdam) **25**, 792 (1959).
[19] J. DeBoer, J. M. J. Van Leuwen, and J. Groeneveld, Physica (Amsterdam) **30**, 2265 (1964).
[20] M. Baus and J. Hansen, Phys. Rep. **59**, 1 (1980).
[21] J. P. Hansen, G. M. Torrie, and P. Vieillefosse, Phys. Rev. A **16**, 2153 (1977).
[22] T. Taguchi, T. Yasunami, and K. Mima, Phys. Rev. A **45**, 3913 (1992).
[23] F. J. Rogers, Phys. Rev. A **29**, 868 (1984).
[24] V. Schwarz, Th. Bornath, W.-D. Kraeft, S. H. Glenzer, A. Höll, and R. Redmer, Contrib. Plasma Phys. **47**, 324 (2007).
[25] V. Bezkrovniy, M. Schlanges, D. Kremp, and W.-D. Kraeft, Phys. Rev. E **69**, 061204 (2004).
[26] G. Kelbg, Ann. Phys. **12**, 219 (1964).
[27] G. Kelbg, Ann. Phys. **12**, 354 (1964).
[28] C. Deutsch, Phys. Lett. **60A**, 317 (1977).
[29] Yu. L. Klimontovich and W.-D. Kraeft, High Temp. Phys. (USSR) **12**, 212 (1974).
[30] J. Vorberger, M. Schlanges, and W.-D. Kraeft, Phys. Rev. E **69**, 046407 (2004).
[31] W. R. Magro, D. M. Ceperley, C. Pierleoni, and B. Bernu, Phys. Rev. Lett. **76**, 1240 (1996).
[32] B. Militzer and D. M. Ceperley, Phys. Rev. Lett. **85**, 1890 (2000).
[33] A. V. Filinov, M. Bonitz, and Yu. E. Lozovik, Phys. Rev. Lett. **86**, 3851 (2001).
[34] O. Pfaffenzeller, D. Hohl, and P. Ballone, Phys. Rev. Lett. **74**, 2599 (1995).
[35] J. Vorberger, I. Tamblyn, B. Militzer, and S. A. Bonev, Phys. Rev. B **75**, 024206 (2007).
[36] L. Ornstein and F. Zernike, Proc. K. Ned. Akad. Wet. **17**, 793 (1914).
[37] J. F. Springer, M. Pokrant, and F. Stevens, Jr., J. Chem. Phys. **58**, 4863 (1973).
[38] W. H. Press, S. A. Teukolsky, W. T. Vetterling, and B. P. Flannery, *Numerical Recipes* (Cambridge University Press, Cambridge, England, 1994).
[39] T. Morita, Prog. Theor. Phys. **22**, 757 (1959).
[40] W.-D. Kraeft, J. Vorberger, D. O. Gericke, and M. Schlanges, Contrib. Plasma Phys. **47**, 253 (2007).
[41] K. Huang, *Statistical Mechanics* (Wiley, New York, 1987).
[42] C. Deutsch, M. Gombert, and H. Minoo, Phys. Lett. **66A**, 381 (1978).
[43] C. Deutsch, M. Gombert, and H. Minoo, Phys. Lett. **72A**, 481 (1979).
[44] J. Chihara, J. Phys. F: Met. Phys. **17**, 295 (1987).
[45] J. Chihara, J. Phys.: Condens. Matter **12**, 231 (2000).
[46] D. B. Boercker and R. M. More, Phys. Rev. A **33**, 1859 (1986).
[47] G. Gregori, A. Ravasio, A. Höll, S. H. Glenzer, and S. J. Rose, High Energy Density Phys. **3**, 99 (2007).